Large Extracellular Vesicles Induce Stronger Prion Infection in Cell Culture than Small Extracellular Vesicles.

Jakub Soukup[1,2], Tibor Moško[1], Sami Kereïche[3], and Karel Holada[1]

[1]Institute of Immunology and Microbiology, First Faculty of Medicine, Charles University, 128 00 Prague, Czech Republic

[2]Department of Genetics and Microbiology, Faculty of Science, Charles University, 128 44 Prague, Czech Republic

[3]Institute of Biology and Medical Genetics, First Faculty of Medicine, Charles University, 128 00 Prague, Czech Republic

Abstract:

Prions are responsible for a number of lethal neurodegenerative and transmissible diseases in humans and animals. Extracellular vesicles, especially small exosomes, have been extensively studied in connection with various diseases. In contrast, larger microvesicles are often overlooked. In this work, we compared the ability of large extracellular vesicles (lEVs) and small extracellular vesicles (sEVs) to spread prions in cell culture. We utilized two cell culture models of prion infection and isolated lEVs by 20,000 × g force and sEVs by 110,000 × g force. The lEV fraction was enriched in β-1 integrin with a vesicle size starting at 150 nm. The fraction of sEVs was depleted of β-1 integrin with a mean size of 79 nm. Both fractions were enriched in prion protein, but the lEVs contained a higher prion-converting activity. In addition, lEV infection led to stronger prion signals in both cell cultures, as detected by cell and western blotting. Our data suggest the importance of lEVs in the trafficking and spread of prions over extensively studied small EVs.

Keywords: Prion, Extracellular Vesicles, Cell Culture

23 ## Introduction:

24 Prion diseases, such as CJD in humans or scrapie and bovine spongiform encephalopathy in animals, are
25 connected with the accumulation of pathologically misfolded prion protein (PrP^{TSE}) in the brains of
26 affected individuals (1). Normal cellular prion protein (PrP^{C}) has various posttranslational modifications,
27 including two potential N-glycosylation sites, which can be recognized by western blotting as three
28 distinct bands (2, 3). PrP^{C} is localized on membranes by a C-terminal GPI anchor (4). Its structure contains
29 three alpha helixes and a short beta-sheet (5, 6). The misfolding of PrP^{C} into PrP^{TSE} can occur sporadically
30 with or without genetic predisposition (1), induced to PrP^{C} by contact with PrP^{TSE} (1). The beta-sheet
31 structure of PrP^{TSE} is resistant (PrPres) to digestion with proteinase K (PK) (7), which could be used to
32 track infection in organs or cell cultures. Prions are most likely transmitted horizontally between
33 individuals by the oral pathway (8). However, how exactly prions spread from the gut to the brain
34 remains unknown. One possible theory described by McBride et al. (9) is that prions could transmit via
35 splanchnic and vagus nerves. Other possible routes are through lymphoid tissue (10) and follicular
36 dendritic cells (11). Intercellular transmission occurs in three possible ways: 1) cell-to-cell contact (12), 2)
37 tunneling nanotubes (13), and 3) EVs (14). Other mechanisms have been proposed, such as trogocytosis
38 or GPI-painting (15, 16).

39 Extracellular vesicles (EVs) are small cell-derived lipid vesicles with significant physiological and
40 pathological functions (17). EVs can be divided into three primary groups depending on their size and
41 biogenesis. Exosomes are generated by endosomal sorting complex required for transport (ESCRT)-
42 dependent (18, 19) and ESCRT-independent pathways (20). The ESCRT-dependent pathway involves the
43 ESCRT mechanism, formed by four distinct heterotrimers (ESCRT-0, ESCRT-I, ESCRT-II, and ESCRT-III) of
44 inward budding in early endosomes generating intraluminal vesicles (ILVs) and maturing early
45 endosomes in multivesicular bodies (MVBs) (18, 19). MVBs can be recycled back to the cell membrane,

46 releasing ILVs as exosomes with sizes of 30–100 nm (18, 21). Another pathway leads MVBs to fuse with
47 lysosomes, degrading ILVs (22, 23). Additionally, MVBs can fuse with autophagosomes, creating
48 amphisomes from which ILVs are released (24, 25). As a result, exosomes contain ESCRT-associated
49 proteins such as TSG-101, tetraspanins (CD9, CD63, CD81), or Alix (through the Syntenin-Alix pathway
50 (26, 27)). An ESCRT-independent pathway utilizes neutral sphingomyelinase (NSMase), which hydrolyzes
51 sphingomyelin to ceramide and induces the aggregation of microdomains to form ILVs (20).
52 Microvesicles (MVs) are vesicles 100–1000 nm in size (18) generated by direct budding from the cell
53 membrane. The budding of MVs is regulated by Cdc42 (a Rho family protein) and its downstream
54 effector Ras GTPase activating-like protein 1 (28). The actin cytoskeleton regulator RhoA is also involved
55 in the dynamics of MV budding (29, 30). ESCRT-I and III mechanisms play roles also in MV biogenesis.
56 Furthermore, ceramide has been reported to be involved in the biogenesis (31, 32). Cone shape-
57 structured tetraspanins are also involved in forming MVs (33). Based on their biogenesis, MVs contain
58 adhesion molecules such as β-1 integrin (34, 35) or Annexin A1 (36). The last primary type of
59 extracellular vesicles is apoptotic bodies, which have variable sizes between 50 and 5000 nm and are
60 generated during apoptosis (35). Apoptotic bodies are enriched with phosphatidylserine on their surface,
61 targeting it for fast phagocytosis by leukocytes (35), which should eliminate them from effective cellular
62 communication (37). Recently, more subpopulations of EVs have been distinguished using various
63 isolation techniques (27, 36, 38, 39).

64 In the cell, PrP^{C} is translocated to the plasma membrane in both nonraft (40) and raft domains (41-43),
65 where it is recycled back by clathrin- or caveolin-1-coated pits to endosomes, from which it can mature
66 into MVBs (40, 44-46). Cytosolic PrP^{C} is prevalent in MVBs (47, 48), with endolysosomal complexes
67 serving as one of the conversion sites for PrP^{TSE} (49, 50). Vilette et al. (51) found that exosomal prion
68 infectivity is associated with both ESCRT-dependent and ESCRT-independent release pathways. The
69 intercellular infectivity of PrP^{TSE} is decreased by blocking NSMase-2, while the PrP^{TSE} content in the cell

70 increases (48, 52). PrP^{TSE} present in exosomes (14) is able to infect neuronal cells both in vitro and in vivo
71 (53). One of the possible physiological roles of PrP^{C} is the mediation of EV transport along neuronal cells,
72 for which PrP^{C} located in EVs hydrophilically interacts with neuronal PrP^{C} located on the plasma
73 membrane (54), which is proposed to be the primary conversion site for PrP^{TSE} (49, 55). From the plasma
74 membrane, PrP^{TSE} is also transported via the endolysosomal pathway (56) to lysosomes (57) and possibly
75 MVBs. As exosomes, PrP^{TSE} on membrane-derived microvesicles is also released from cells (58).

76 PrP^{TSE} is present in plasma EVs of symptomatic and asymptomatic mice infected with prions (59, 60).
77 Thus, via blood transfusion, EVs can contribute to recorded horizontal infection with variant CJD (61).
78 The involvement of EVs in the oral pathway of infection is also possible since EVs can survive the
79 stomach environment (62, 63).

80 In our work, we utilized two cell culture models of prion infection to compare PrP^{TSE} content and prion
81 infectivity in the sEV fraction predominant with exosomes and the lEV fraction predominant with
82 microvesicles. Here, we report that both fractions of EVs are enriched in PrP, but lEVs are able to infect
83 native cells with more efficiency than sEVs.

84 Methods:

85 Materials:

86 Antibodies: From Abcam, we obtained rabbit anti-β-actin (EPR21241), fin. con. 0.25 µg/ml; and mouse
87 anti-Alix (3A9), fin. con. 2 µg/ml. From Azure Biosystems, we obtained goat anti-mouse AzureSpectra 700
88 or 800 conjugate, fin. con. 0.4 µg/ml; and goat anti-rabbit AzureSpectra IR700 or IR800 conjugate, fin.
89 con. 0.4 µg/ml. From Enzo Life Sciences, we obtained rabbit anti-HSP70/HSC70 (ADI-SPA-797), fin. con. 1
90 µg/ml; and rabbit anti-calnexin (ADI-SPA-865), fin. con. 1 µg/ml. From Santa Cruz Biotechnology, we
91 obtained rabbit anti-β1 integrin (M-106), fin. con. 2 µg/ml; goat anti-TSG-101 (M-19), fin. con. 2 µg/ml;

92 and rabbit anti-CD63 (H-193), fin. con. 2 µg/ml. Mouse anti-PrP (6D11), fin. con. 0.5 µg/ml was obtained
93 from Biolegend, mouse anti-CD9 (MM2/57), fin. con. 0.5 µg/ml was obtained from Merck; mouse anti-
94 PrP (AH6), fin. con. 0.5 µg/ml was obtained from The Roslin Institute, and donkey anti-mouse Alkaline
95 Phosphatase conjugate, fin. con. 0.3 µg/ml was obtained from Jackson ImmunoResearch.

96 ## Cells:

97 Prion infection models were used in the CAD5 cell line (originated from: RRID:CVCL_0199)(64), the N2a-
98 PK1 cell line (RRID:CVCL_WI10)(65), and cells chronically infected with the RML5 prion strain (CAD5-RML,
99 N2a-PK1-RML). The cells were maintained in Opti-MEM (Thermo Fisher Scientific) supplemented with
100 10% bovine growth serum (BGS, HyClone Bovine Growth Serum, GE Healthcare Life Sciences) and 100 U
101 of penicillin/streptomycin/ml (Lonza). CAD5 cells were passaged by washing with 0.5 mM EDTA in PBS
102 followed by resuspension in fresh medium. The N2a-PK1 cell line was passaged by washing with 0.5 mM
103 EDTA in PBS and trypsinized (Trypsin-EDTA 0.25%, Thermo Fisher Scientific).

104 All relevant data on EV production, isolation, and characterization were submitted to the EV-TRACK
105 knowledgebase (EV-TRACK ID: EV220318)(66). For EV production, the cells were passaged a day before
106 production (~ 30% confluence). Cells were washed with PBS (Lonza), and Exo-free Opti-MEM was added
107 for conditioning with EVs. The exo-free Opti-MEM medium was produced as published (67). Opti-MEM
108 supplemented with 20% BGS and penicillin/streptomycin was centrifuged at 110,000 × g (SW28 rotor,
109 Beckman) for 20 hours at 4 °C in an ultracentrifuge (LE-80K, Beckman). The centrifuged medium was
110 diluted with serum-free Opti-MEM supplemented with penicillin/streptomycin to a final concentration of
111 10% BGS and filtered using the Stericup-VP Sterile Vacuum Filtration System with a 0.1 µM PES filter
112 (Merck). The cells were incubated with the medium for 48 hours. When the conditioned medium was
113 harvested, the cells had 100% confluence with a minimum of dead/floating cells.

114 ## Isolation of EVs:

115 EVs were isolated from the conditioned medium by a series of differential centrifugations. All steps were
116 performed on ice, and samples were centrifuged at 4 °C. The conditioned medium was centrifuged at
117 300 × g for 15 min. The supernatant was collected and centrifuged at 2,000 × g for 20 min to sediment
118 large cell debris. The supernatant was centrifuged at 10,500 rpm (~20,000 × g) for 70 min (SW28 rotor,
119 Beckman). Pelleted lEVs were resuspended in 13.5 ml of PBS (Lonza) and sedimented again at 10,500
120 rpm (~20,000 × g) for 70 min (SW40 rotor, Beckman). The supernatant containing sEVs was centrifuged
121 at 25,000 rpm (~ 110,000 × g) for 70 min (SW28 rotor). The pellet was resuspended in ~ 12 ml of PBS and
122 underlaid with 2 ml of 40% sucrose in 0.2 M Tris-HCl pH 7.4 and centrifuged under the same conditions.
123 The sucrose cushion containing sEVs was collected with an 18 G needle, diluted with PBS to a final
124 volume of 13.5 ml, and centrifuged again. Both lEVs and sEVs were resuspended in PBS and frozen on dry
125 ice. Pure EVs were used for western blot characterization and infection using fractions standardized to
126 the same amount of protein determined by the BCA assay (Pierce BCA assay kit, Thermo Fisher
127 Scientific). The graphical scheme of isolation is shown in Fig. 1.

128 ## Infection of cells:

129 Native cells were passaged 24 h before infection. The cells were washed with 5 ml of PBS, and an Exo-
130 free medium containing isolated EVs was added for ~ 72 h. Two schemes of cell infection were used. In
131 the first scheme, lEVs and sEVs were standardized according to the original volume of the collected
132 sample. We abbreviated this scheme as OVS (Original Volume Standardization). The pelleted lEVs after
133 the first 20,000 × g spin and sEVs after the first 110,000 × g spin were resuspended in a volume of Exo-
134 free medium that was identical to the starting volume of the collected conditioned medium (8 ml).
135 Aliquots of 4, 2, and 1 ml were used to infect native cells in a 25 cm^2 flask or 100 µl in a 96-well plate. The
136 second infection scheme was standardized to contain the same amount of total protein used to infect
137 cells. We use TPS (Total Protein Standardization) as an abbreviation. Cells in a 25 cm^2 flask were infected

138 with 10, 5, or 2.5 µg of total protein in EV fractions. On a 96-well plate, the cells were infected with 0.2,

139 0.1, or 0.05 µg of EV fractions. The cells were passaged every 3-4 days to reach the 10th or 12th passage.

140 Two independent experiments, including EV production and isolation, were carried out. As a positive

141 control, the cell homogenates of RML-infected cells were used, and negative controls were homogenates

142 of the noninfected cells. The graphical scheme of infection is shown in Fig. 1.

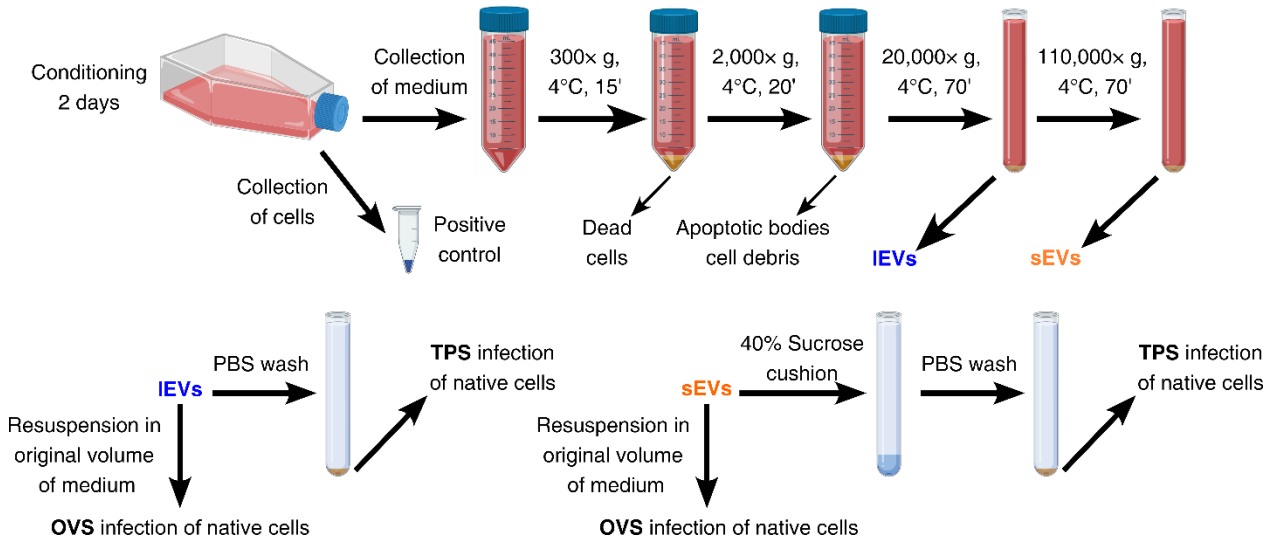

143

144 **Figure 1: Scheme of lEV and sEV isolation and infection of native cells by the OVS and TPS.** Created with BioRender.com

145 ## Harvesting of the cells after the infection for analysis:

146 CAD5 or CAD5-RML cells were resuspended in 0.5 mM EDTA in PBS by pipetting. N2a-PK1 or N2a-PK1-

147 RML cells were washed in 0.5 mM EDTA in PBS. The cells were centrifuged at 300 × g and 4 °C for 10 min,

148 the supernatant was discarded, and the pellets were frozen at -80 °C. The pellets were thawed on ice,

149 and freeze–thaw cycles were performed 3 times in total. The cells were homogenized using a 30 G

150 needle. To determine the protein concentration, part of the homogenate was lysed in lysis buffer (150

151 mM NaCl, 50 mM Tris-HCl pH 7.5, 0.5% (V/V) Triton X-100, 0.5% (w/V) sodium deoxycholate) along with

152 part of the collected EVs. The samples were incubated on ice for 30 min with occasional vortexing and

153 then centrifuged at 14,000 × g and 4 °C for 10 min. The supernatant was used to determine the protein

154 concentration by BCA assay according to the manufacturer's instructions (Pierce BCA Protein Assay Kit,
155 Thermo Fisher Scientific).

156 Cell blot:

157 All steps were performed at room temperature unless stated otherwise. Infected cells were seeded in
158 duplicate on a plastic coverslip in a 24-well plate and grown to confluency, as we published previously
159 (68). The coverslips were blotted on a 0.45 µm nitrocellulose membrane (Bio-Rad) wetted in lysis buffer.
160 The membranes were dried and incubated in lysis buffer containing 7 µg/ml proteinase K (PK, Sigma–
161 Aldrich) at 37 °C for 90 min. The membranes were washed 2× in Milli-Q H_2O (MQH_2O). The PK was
162 stopped with 2 mM phenylmethylsulfonyl fluoride (PMSF) in PBS for 10 min and washed 3× in MQH_2O.
163 The membranes were denatured with 3 M guanidium thiocyanate in 10 mM Tris-HCl pH 7.5 for 10 min
164 and washed with MQH_2O 5×. After denaturation, membranes were blocked in 5% nonfat milk in 0.5%
165 Tween in Tris buffer pH 7.4 (TBS-T) for 30 min. The primary antibodies anti-PrP 6D11 and AH6 were
166 diluted in a blocking solution, and the membranes were incubated for 2 h at RT or overnight at 4 °C with
167 antibodies. Membranes were washed with TBS-T 3× 5 min and incubated in secondary antibody
168 conjugated to alkaline phosphatase diluted in blocking solution for 1 h. The membranes were washed
169 with TBS 5× 5 min and developed using BCIP/NTP (Merck). The reaction was stopped using MQH_2O.
170 Densitometry was evaluated in AzureSpot software (v.2.0, Azure Biosystems) on background-corrected
171 images. Data are presented as the mean with standard error of the mean (SEM).

172 SDS–PAGE and western blot:

173 The frozen cell pellets were thawed on ice, resuspended in lysis buffer, and incubated on ice for 30 min
174 with occasional vortexing. Lysed cells were centrifuged at 14,000 × g at 4 °C for 10 min. The collected
175 supernatant was used to measure protein concentration using the BCA assay (Pierce BCA Protein Assay
176 Kit, Thermo Fisher Scientific) according to the manufacturer's instructions. The EVs were thawed on ice,

177 and part was diluted in lysis buffer to measure protein concentration as in cell lysates. Nonlysed EVs
178 were diluted with MQH_2O to unify the protein concentration, and sample buffer was added (final
179 concentration: 0.5 M Tris-HCl pH 6.8, 4% SDS, 0.125% bromophenol blue, 12.5% glycerol). Cell lysates
180 were diluted with MQH_2O to standardize the protein concentration before adding the sample buffer. To
181 detect PrPres, lysates and EVs were incubated with PK (50 µg/ml) at 37 °C for 45 min prior to adding the
182 sample buffer. The samples were boiled at 95 °C for 10 min. Boiled samples were loaded on 10%
183 acrylamide/bisacrylamide gel (Bio-Rad) or TGX Stain-Free™ FastCast™ 12% acrylamide gel (Bio-Rad).
184 Proteins on gels were imaged in an Azure c600 imaging system according to the manufacturer's
185 instructions. Separated proteins on the gels were blotted on Amersham™ Hybond® low-fluorescence 0.2
186 µm PVDF membranes (Merck). The membranes were blocked using fluorescence blocking buffer (Azure
187 Biosystems) at RT for 30 min. Primary antibodies were diluted in blocking buffer and incubated at RT for
188 2 h or at 4 °C overnight on a rocker. The membranes were washed with IR washing buffer (Azure
189 Biosystems) 3× 5 min. Washed membranes were incubated with secondary antibody diluted in blocking
190 buffer at RT for 1 h. Secondary antibodies were washed 3× 5 min in IR washing buffer and 2× 5 min in
191 PBS. After drying, the membranes were imaged using the Azure c600 imaging system. Densitometry was
192 evaluated in AzureSpot 2.0 software using predefined 200-radius rolling ball background subtraction.
193 Data are presented as the mean with SEM.

194 Real-Time Quacking Induced Conversion (RT-QuIC):

195 The collected EV pellets were thawed on ice and homogenized with a 30 G needle, and the protein
196 content was measured by BCA assay. Homogenized cells and EVs were diluted to 3.2 µg/µl using PBS,
197 corresponding to 10% cell homogenate protein content. By decimal and quintuple dilutions, EVs and cell
198 homogenate were diluted to 10^{-6} – 10^{-9} and 10^{-5} – 3×10^{-11}, respectively, in PBS buffer containing 1× N-2
199 supplement (Gibco, Thermo Fisher Scientific) and 0.1% SDS and then analyzed by second-generation RT-
200 QuIC assay. All samples were run in quadruplicate in a Nunc™ MicroWell™ 96-Well Optical-Bottom Plate

201 (Thermo Fisher Scientific). Each well contained reaction mix (10 mM phosphate buffer, pH 7.4; 300 mM
202 NaCl; 10 µM thioflavin T (ThT); 1 mM EDTA; 0.002% SDS; and 0.1 mg/ml rSHa PrP (90–231)) and 2 µL of
203 sample in a volume of 100 µL. The reaction was carried out using the FLUOstar Omega plate reader
204 (BMG LABTECH GmbH), undergoing repeating shaking cycles of 60 s (700 rpm, double orbital) and 60 s of
205 rest for 60 h at 55 °C. Fluorescence was measured every 15 min. Each test was analyzed using Mars
206 software (BMG LABTECH GmbH) (69, 70).

207 ## Cell Scrapie Assay:

208 All steps were performed at room temperature unless stated otherwise, as previously published (71).
209 Infected CAD5 cells were seeded in ELISPOT plates (multiscreen 96-well filter plates with high protein-
210 binding Immobilon-P membrane, 0.45 µm, Millipore) activated with 70% ethanol. Ethanol was removed
211 by vacuum (Supelco), and the wells were washed 2× with PBS. Cells (1,000, 5,000, or 10,000 per well)
212 were transferred to the plates, immobilized on the membrane using a vacuum, and dried at 50 °C. The
213 dried plates were incubated with 60 µl of PK (2 µg/µl) in lysis buffer at 37 °C for 30 min. PMSF (2 mM)
214 was added in PBS to inhibit PK for 10 min. Cells were washed with PBS, and proteins were denatured
215 with 3 M guanidium thiocyanate in 10 mM Tris-HCl pH 7.5 for 10 min and washed 4× with PBS. The
216 membranes were blocked using Superblock™ solution (Thermo Fisher Scientific) for 1 h. After blocking,
217 the membranes were incubated with 6D11 primary antibody diluted in Superblock™ solution at 4 °C
218 overnight. The primary antibody was washed away 4× with TBS-T, and the membranes were incubated
219 with a secondary antibody conjugated with alkaline phosphatase diluted in Superblock™ solution for 1 h.
220 The secondary antibody was washed away 5× with TBS-T and developed with an AP Conjugate Substrate
221 Kit (Bio-Rad). Spots were quantified using a Nikon ELISPOT system and NIS-Elements AR software (v.
222 4.20). GraphPad Prism 5 (v. 5.03, GraphPad Software) was used for statistical analysis. Infections with
223 lEVs were compared to corresponding sEV infections using a two-tailed unpaired t test (data passed the

224 D'Agostino and Pearson omnibus normality test and the Shapiro–Wilk normality test). Data are
225 presented as the mean with SEM.

226 Electron Microscopy:

227 For transmission electron microscopy (TEM), EM grids (FCF200-Cu, Electron Microscopy Sciences) were
228 prepared as published (67, 72). Isolated EVs were diluted 10× in PBS. Grids were incubated for 20 min on
229 a 15 µl drop of EV suspension and transferred to a 50 µl drop of 4% formaldehyde in PBS for another 20
230 min. The fixed samples were washed on a 100 µl drop of PBS and fixed again on a 50 µl drop of 1%
231 glutaraldehyde in PBS (electron microscopy grade, Sigma–Aldrich) for 5 min. The grids were washed 8×
232 on a 100 µl drop of MQH_2O. Washed grids were contrasted on 25 µl drops of uranyl oxalate pH 7 for 5
233 min. Contrasted grids were transferred on 25 µl drops on ice of a mix of 4% uranyl acetate and 2%
234 methylcellulose (1:9) for 10 min. The mix was slowly removed with filter paper, and the grid was air-
235 dried. Cryo-TEM samples were prepared by plunge freezing (72, 73). The EV sample (3 µl) was applied to
236 Lacey carbon grids (LC-200 Cu, Electron Microscopy Sciences) covered with a perforated carbon film and
237 discharged for 40 s with a 5 mA current. Most of the sample was removed by blotting (~ 1 s), and the
238 sample was immediately plunged into liquid ethane kept at -183 °C. The grids were transferred without
239 reheating to a Gatan 626 cryo-specimen holder and imaged in a Tecnai G2 Sphera 20 transmission
240 electron microscope equipped with a LaB6 gun and a Gatan UltraScan 1000 slow-scan CCD camera. The
241 images were recorded at an accelerating voltage of 120 kV. All pictures were CTF-corrected and
242 bandpass filtered to suppress ice thickness and noise below 1 nm detail size.

243 Results:

244 Characterization of lEV and sEV fractions

245 The isolated fractions of lEVs and sEVs from CAD5-RML and N2a-PK1-RML cells differed in protein
246 composition (Figs. 2A and B). Common markers for EVs, Alix, HSP70, TSG-101, CD63, and CD9, were

247 present in both fractions of EVs. In contrast, we did not detect calnexin, a marker of contamination by
248 the endoplasmic reticulum, in our EV fractions. In the CAD5-RML lEV fraction, very weak bands were
249 detected by calnexin antibody (Fig. 2C). To distinguish lEVs from sEVs, we used β-1 integrin as a marker
250 (Fig. 2C). Large EVs, which should consist mainly of MVs generated by budding from the plasma
251 membrane, should be enriched in this marker compared to sEVs. In CAD5-RML cell line, we isolated sEVs
252 depleted of β-1 integrin (Fig. 2C), but sEVs from N2a-PK1-RML cell line were not completely depleted of
253 β-1 integrin (Fig. 2D). The sEV fractions were enriched in the tetraspanin markers CD9 and CD63, TSG-
254 101, and Alix compared to the lEVs in both cell lines. The presence of EVs in isolated fractions was
255 verified by electron microscopy. As shown in Figs. 2E and F, CAD5 lEVs and sEVs differed in size. The size
256 difference was also visible in the N2a-PK1 cell line (Figs. 2G and H), although in sEVs, the vesicles were
257 larger compared to CAD5 cell sEVs. In addition, we used cryo-electron microscopy to visualize the
258 ultrastructure of CAD5 lEVs and sEVs where lipid bilayers were visible (Fig. 2I-L). We found that the mean
259 size (n = 200) of sEVs was 79 nm (SEM ±3 nm). The largest vesicles in the sEV fraction were
260 approximately 150 nm in diameter. The sizes of the visible vesicles in the lEV fraction ranged from ~100
261 nm – ~500 nm. Larger vesicles were present but deformed due to the thickness of the ice or holes in the
262 perforated carbon film (Fig. 2I).

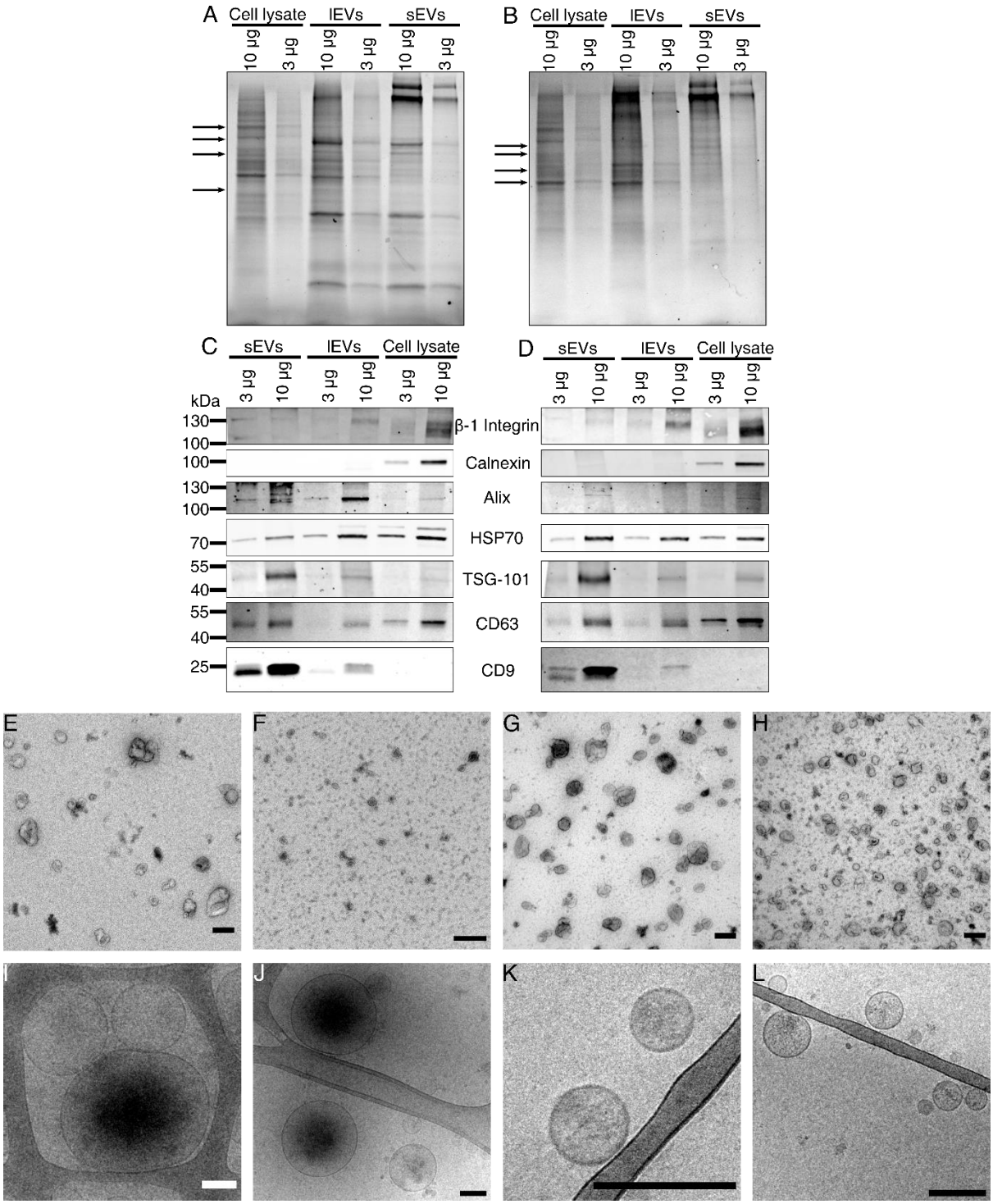

Figure 2: Characterization of lEV and sEV fractions. (a,b) An example images of the TGX Stain-Free™ SDS–PAGE protein profile of CAD5-RML (a) or N2a-PK1 (b) cell lysate, lEVs, and sEVs with the loading of 3 µg or 10 µg of proteins in line. Arrows point to examples of protein profile differences between cell lysate, lEVs, and sEVs. (c,d) An example of images of the detection of markers in the EV fraction from the CAD5-RML (c) or N2a-PK1-RML (d) cell line. β-1 integrin: marker of lEVs; calnexin: endoplasmic reticulum marker – contamination of EV fractions; Alix, HSP-70, TSG-101, CD63 and CD9: common markers for sEVs and lEVs. (e-g) An example images of EVs present in the lEV (e, g) and sEV (f, h) fractions isolated from CAD5 (e, f) or N2a-PK1 (g,

h) cells contrasted with uranyl oxalate. Bars: 200 nm. (i-l) Cryo-electron microscopy images of vesicles in lEV (i, j) and sEV (k, l) fractions from CAD5 cells. Bars: 200 nm. For visualization purposes, all images were enhanced with brightness and contrast.

Large and small EVs are enriched in PrP^{C} and PrP^{res} content compared to intact cells.

We found that PrP in both EV fractions was greatly enriched compared to the whole-cell lysates of corresponding cell lines (Figs. 3A-D). When PrPres was normalized to whole-cell lysate PrP PK- (PrP^{C} + PrP^{Sc}), we found that in lEVs, there was approximately five times more PrP^{res} in CAD5-RML cells and approximately 18 times more PrPres in N2a-PK1-RML cells. In sEVs, there were approximately 8 and 11 times more PrPres than in the cell lysates of CAD5-RML cells and N2a-PK1-RML cells, respectively. There was approximately 5× less PrPres in whole-cell lysate compared to PrP PK- in CAD5-RML cells and approximately 20× less in N2a-PK1 cells. While the amount of PrPres was slightly higher (1.5×) in lEVs than in sEVs from N2a-PK1-RML cells, the amount of PrP^{res} in lEVs from CAD5-RML cells was slightly lower than that in sEVs (Fig. 3E). Similar patterns were also recorded for the amounts of PrP PK- in the EV fractions in the CAD5-RML and N2a-PK1-RML cell lines (Fig. 3F).

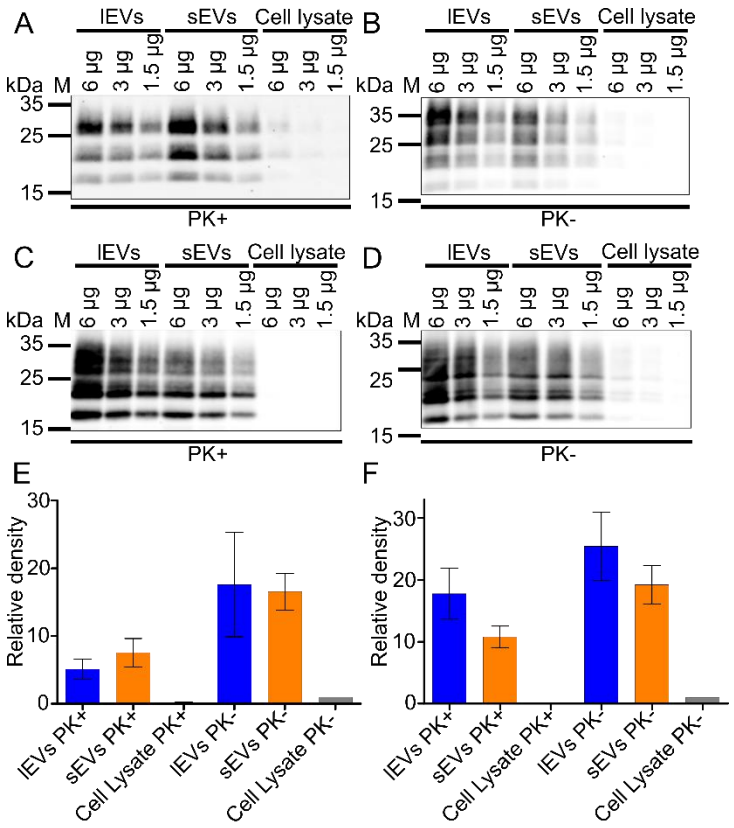

284 **Figure 3: western blot analysis of PrP levels in EV fractions.** (a-d) CAD5-RML (a, b) or N2a-PK1-RML (c, d) lEVs, sEVs, and whole-
285 cell lysate were treated with proteinase K (PK+, a, c), and PrPres was detected using a mix of prion antibodies 6D11 and AH6.
286 Untreated (PK-) samples (b, d) demonstrated the presence of total PrP (PrP^{C} + PrP^{Sc}). For visualization purposes, all images were
287 enhanced with brightness and contrast. (e,f) Comparison of the relative densities of PrPres bands in lEVs, sEVs, and whole-cell
288 lysate normalized to PrP PK- signal in whole-cell lysate from CAD5-RML (e) or N2a-PK1-RML (f) cells. Bars represent the mean
289 with SEM of biological triplicates, each with technical triplicates (3 different protein loadings on gel – 6, 3, or 1.5 µg per line).
290

291 ## Large EVs have higher prion-converting activity than small EVs.

292 We used an endpoint dilution RT-QuIC assay to determine the prion-converting activity in the EV
293 fractions standardized to contain the same amount of total protein. The seeding dose 50 (SD_{50}) of CAD5-
294 RML lEVs was twenty times higher than that of sEVs (2×10^{-8} vs. 4×10^{-7}, Fig. 4E). Additionally, the
295 maximum relative fluorescence at a 10^{-5} dilution was higher and the lag phase shorter in lEVs (163,000
296 and 390 min, Fig. 4A) than in sEVs (151,000 and 480 min, Fig. 4B). In N2a-PK1-RML cells, the difference
297 was less convincing. In the first experiment, there was approximately 26× higher prion-converting
298 activity in lEVs (SD_{50}: 3×10^{-9} vs. 8×10^{-8}) and the maximum relative fluorescence and lag phase of the 10^{-5}
299 dilution were 184,000 and 570 min for lEVs and 119,000 and 855 min for sEVs, respectively (Fig. 4C and
300 D). In the second experiment, no difference was recorded (SD_{50}: 3×10^{-9} vs. 3×10^{-9}) and the respective
301 values were 152,000 and 735 in lEVs and 146,000 and 690 in sEVs of the 10^{-5} dilution. The numbers of
302 positive wells in quadruplicate for each sample and dilution are summarized in Supplementary Table S1.

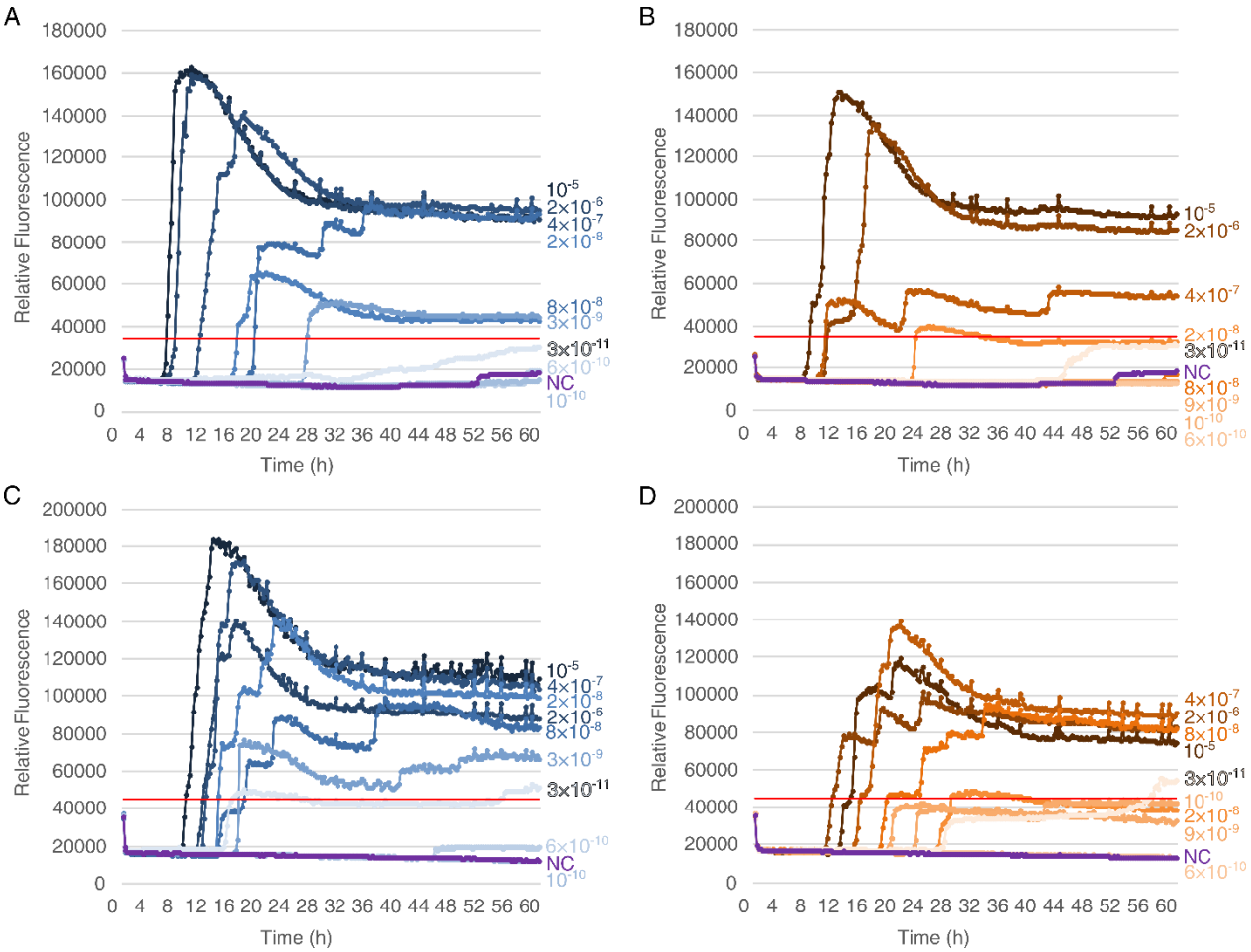

E

Seeding Dose 50			
Sapmle	lEVs	sEVs	Whole cell lysate
CAD5-RML 1st experiment	10^{-8}	10^{-6}	10^{-8}
CAD5-RML 2nd experiment	2×10^{-8}	4×10^{-7}	
PK1-N2a-RML 1st experiment	3×10^{-9}	3×10^{-9}	
PK1-N2a-RML 2nd experiment	3×10^{-9}	8×10^{-8}	

Figure 4: Comparison of EV fractions' prion converting activity using endpoint dilution RT-QuIC assay. (a-d) Quintuple dilution series of CAD5-RML lEVs (a), CAD5-RML sEVs (b), N2a-PK1-RML lEVs (c), and N2a-PK1-RML sEVs (d). Each line in the graphs represents the mean value of the technical quadruplicate. Redline – threshold (mean plus 5× standard deviation from negative control). NC (purple line) – negative control (uninfected CAD5 or N2a-PK1 whole cell lysate at 10^{-5} dilution, corresponding to 0.001% cell homogenate). (e) Table with seeding dose 50 from two independent experiments. The value represents the highest dilution, where at least 2 out of 4 technical replicates gave positive results.

A fraction of lEVs is more effective in the infection of cultured cells than a fraction of sEVs.

After fraction characterization, we infected native CAD5 or N2a-PK1 cells with EVs isolated from the corresponding chronically infected cells. First, we infected native CAD5 cells with supernatants collected

314 during EV isolation (Supplementary Fig. S1) to monitor the loss of infectivity produced by individual
315 centrifugation steps. Most of the infectivity was lost after pelleting floating cells (300 × g). The next
316 visible loss of infectivity occurred after pelleting of the lEVs. Some infectivity remained in the
317 conditioned medium even after pelleting sEVs (110,000 × g supernatant) as demonstrated by visible
318 infection of the cells after 10 passages (Supplementary Fig. S1F). The results from supernatant infection
319 were in agreement with the infection with collected pellets during the isolation procedure
320 (Supplementary Fig. S2). We compared cell blots of infected cells with lEVs and sEVs in passages 3, 5, 8,
321 and 10 (Fig. 5A-D). We found that lEVs infected native cells more effectively than sEVs in both cell lines.
322 We used two schemes of infection: an OVS (original volume standardization) reflects the total amount of
323 prion infectivity associated with the isolated EV fractions, and a TPS (total protein standardization)
324 reflects the concentration of prion infectivity present in the isolated EV fractions. The differences in cell
325 blot by OVS infections were uniform during the passages after infection of CAD5 cells. Infection by lEVs
326 was 1.5× - 2.3× stronger (1.7×, 1.5×, 1.5× and 2.3× in passages 3, 5, 8, and 10, respectively, Figs. 5E - H).
327 Similarly, infection by lEVs was stronger in TPS infection. In earlier passages, the difference was smaller.
328 In passage 3, lEV infection was 1.4× stronger, and in passage 5, it was 1.6× stronger. In later passages 8
329 and 10, the infection was 4.1× stronger (Figs. 5E – H). In the N2a-PK1 cell model, stronger infection by
330 lEVs was confirmed. The OVS led to 1.4× - 1.7× stronger infection by lEVs (1.7×, 1.4×, 1.5× and 1.4× in
331 passages 3, 5, 8, and 10). In the TPS scheme of infection, lEVs infected N2a-PK1 cells 1.2× more strongly
332 in all passages, except for passage 5, where the infection by lEVs was weaker than that by sEVs (Figs. 5E –
333 H). The absolute values of the measured densities are shown in Supplementary Fig. S3.

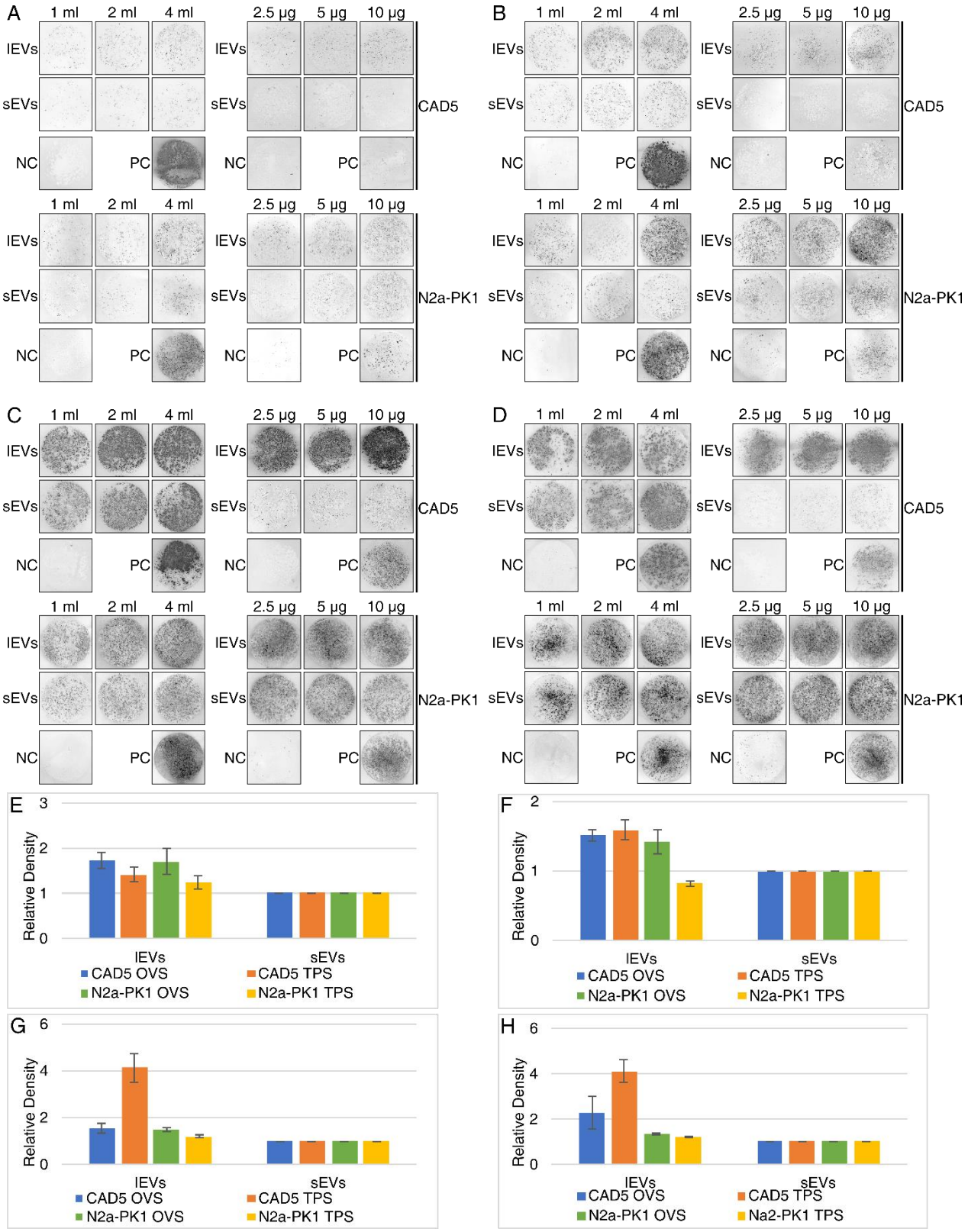

Figure 5: Example images of cell blots from passages after infection with lEVs and sEVs with densitometry analysis. (a-d) Example images of cell blots from infection of native CAD5 or N2a-PK1 cells infected with lEVs and sEVs in different passages

after infection. Cells were infected with 4 ml, 2 ml, and 1 ml of resuspended EVs in OVS infection or with 10 µg, 5 µg, and 2.5 µg of EVs in TPS infection. NC – negative control, PC – positive control. Passages 3 (a), 5 (b), 8 (c), and 10 (d) after infection. For visualization purposes, all images were enhanced with brightness and contrast. (e-h) Densitometry analysis of cell blots from different passages. Infection with lEVs was compared to the corresponding infection with sEVs. Bars represent the fold change in the density of lEVs compared to sEVs. Passages 3 (e), 5 (f), 8 (g), and 10 (h) after infection.

After cell blot analysis, we confirmed the results with western blotting from each passage and infection (Fig. 6 and Supplementary Figs. S4 – S6). From the same samples, western blot analysis showed that infection of CAD5 cells by lEVs was even stronger compared to cell blot analysis. With the OVS scheme, the PrPres signal from lEV-infected CAD5 cells was 1.5× - 3.6× stronger then from sEV-infected CAD5 cells (1.5×, 3.6×, 3.2×, and 1.9× in passages 3, 5, 8, and 10, Fig. 6E and Supplementary Figs. S4-6). TPS infection by lEVs in CAD5 cells led to a much higher PrPres signal in the CAD5 cell model than infection with sEVs. The PrPres signal reached its maximum (where the dilutions had minimal differences) in passage 8, but infection by sEVs just started to appear (Fig. 6C). Within these limitations, we measured a 24.6× stronger PrPres signal in passage 8. Since lEV infection reached its maximum and infection by sEVs continued to increase, the difference dropped to 7.0× and 10.6× in passages 10 and 12, respectively (Supplementary Fig. S6E). In the N2a-PK1 cell line, the trend of stronger infection by lEVs was similar. Unlike CAD5 cells, differences in TPS infection were smaller than in OVS infection in N2a-PK1 cells. TPS infection led to 1.4× - 1.8× stronger PrPres signals in lEV-infected cells than in sEV-infected cells (Fig. 6E and Supplementary Figs. S4-6). In earlier passages of the OVS scheme of infection, the PrPres signal was 2.0× and 1.9× stronger in infections by lEVs in passages 3 and 5, respectively (Supplementary Figs. S4 – S6). Later passages after infection by lEVs revealed a 4.8× stronger PrPres signal in passage 8 and a 3.0× stronger signal in passage 10 (Fig. 6E and Supplementary Fig. S6). The absolute density values for each sample are summarized in Supplementary Figures S7 and S8. As controls, we compared the total PrP signal of non-digested PrP PK- samples in the same manner as PrPres (Fig. 6F). Despite the different strengths of infection by lEVs and sEVs, cells infected by both types of EVs retained similar levels of PrP PK-. The lowest PrP PK- the ratio of lEVs/sEVs (0.96×) was in passage 5 with OVS of CAD5 cells (Supplementary Fig. S5F). The highest ratio of 1.84× was in the 10th passage with OVS of N2a-PK1 cells (Supplementary Fig.

364 6F). As a loading control for PrP PK-, β-actin was used (Fig. 6G). Relative densities of β-actin bands were

365 similar or higher in samples infected with sEVs than with lEVs, confirming that the higher PrPres signal

366 was not caused by elevated protein load.

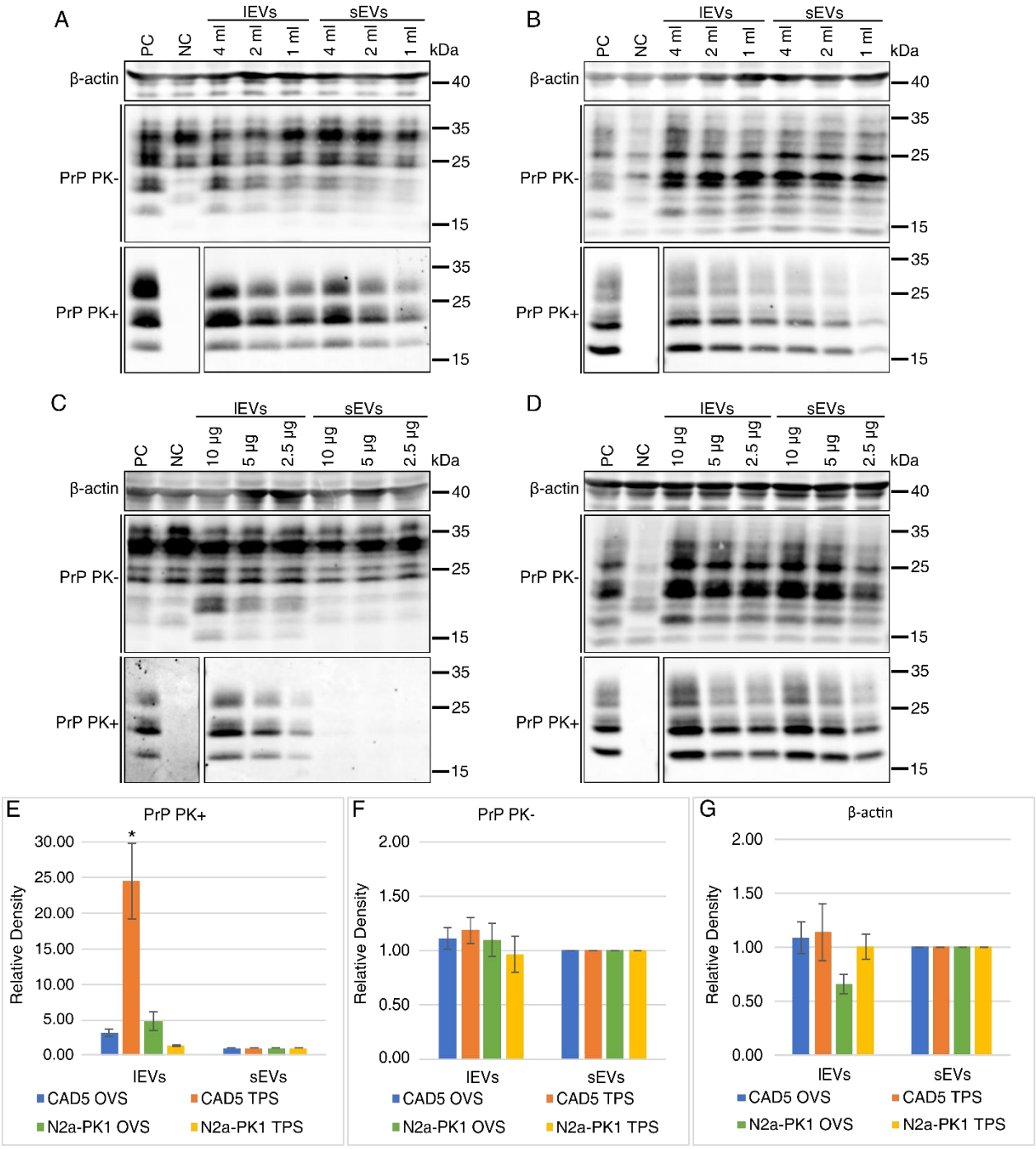

367

368

369 **Figure 6: western blot analysis of PrPres and PrPSc/PrPc signals in cells infected by lEV and sEV fractions at passage 8.** (a-d) An
370 example images of western blots from infection of CAD5 (a, c) or N2a-PK1 (b, d) cells with lEVs and sEVs at passage 8 after
371 infection. Cells were infected with 4 ml, 2 ml, and 1 ml of resuspended EVs in OVS infection (a, b) or with 10 µg, 5 µg, and 2.5 µg
372 of washed EVs in TPS infection (c, d). PK+ - proteinase K digested samples. β-Actin was used as a loading control for PrP PK-
373 samples, which were also compared. Both PrP PK- and PrP PK+ samples are shown for a loading of 40 µg per line. NC – negative
374 control (mock infected cells), PC – positive control. For visualization purposes, all images were enhanced with brightness and
375 contrast. (e) Relative comparison of PrP signal in PrP PK+ samples by densitometry. Bars represent fold change in the density of
376 lEVs compared to the corresponding density in infection of sEVs. Bars show the mean with SEM value of relative differences
377 between lEV and sEV infections from a biological duplicate of EV isolation, a triplicate of infection, and a technical triplicate of
378 sample loading. * PrPres signal reached its maximum in lEV infection and in sEV, infection just started to appear. The
379 quantification precision is limited. (f) Relative comparison of PrP PK- densitometry. (g) Relative comparison of β-actin
380 densitometry.
381
382 As another validation method, we used the standard scrapie cell assay (SSCA) to quantify infection for
383 CAD5 cells precisely. The infections were carried out in hexaplicates for two independent EV isolations
384 (Figs. 7 A, B, E, F, I, and J). In SSCA, dilutions in the TPS scheme reached their maximum level of infection
385 in passage 8. We found a significant difference in passage 5. The mean spot counts (± SEM) in the 0.2 µg
386 infection were 250 ± 20 spots for lEVs and 188 ± 18 spots for sEVs ($p = 0.0309$). At 0.1 µg, there were 206
387 ± 23 spots for lEVs and 113 ± 12 spots for sEVs ($p = 0.0016$) (Fig. 7G). The differences were insignificant in
388 passages 3 (Fig. 7C) and 8 (Fig. 7K). The mean spot counts (± SEM) for lEVs in passage 8 were 553 ± 18,
389 520 ± 16, and 353 ±34 for 0.2, 0.1, and 0.05 µg of total protein, respectively. In sEVs, infection yielded
390 452 ± 48 spots in 0.2 µg, 433 ± 37 in 0.1 µg, and 322 ± 52 in 0.05 µg infection. In the OVS infection, we
391 found significant differences in passage 3 (Fig. 7D) and passage 8 (Fig. 7L) but not in passage 5 (Fig. 7H).
392 The mean spot counts were 511 ± 56 for lEVs and 267 ± 69 for sEVs ($p = 0.0054$, Fig. 7L) for passage 8. In
393 passage 3, the mean spot counts were 163 ± 17 for lEVs and 76 ± 12 for sEVs ($p = 0.0004$, Fig. 7D).

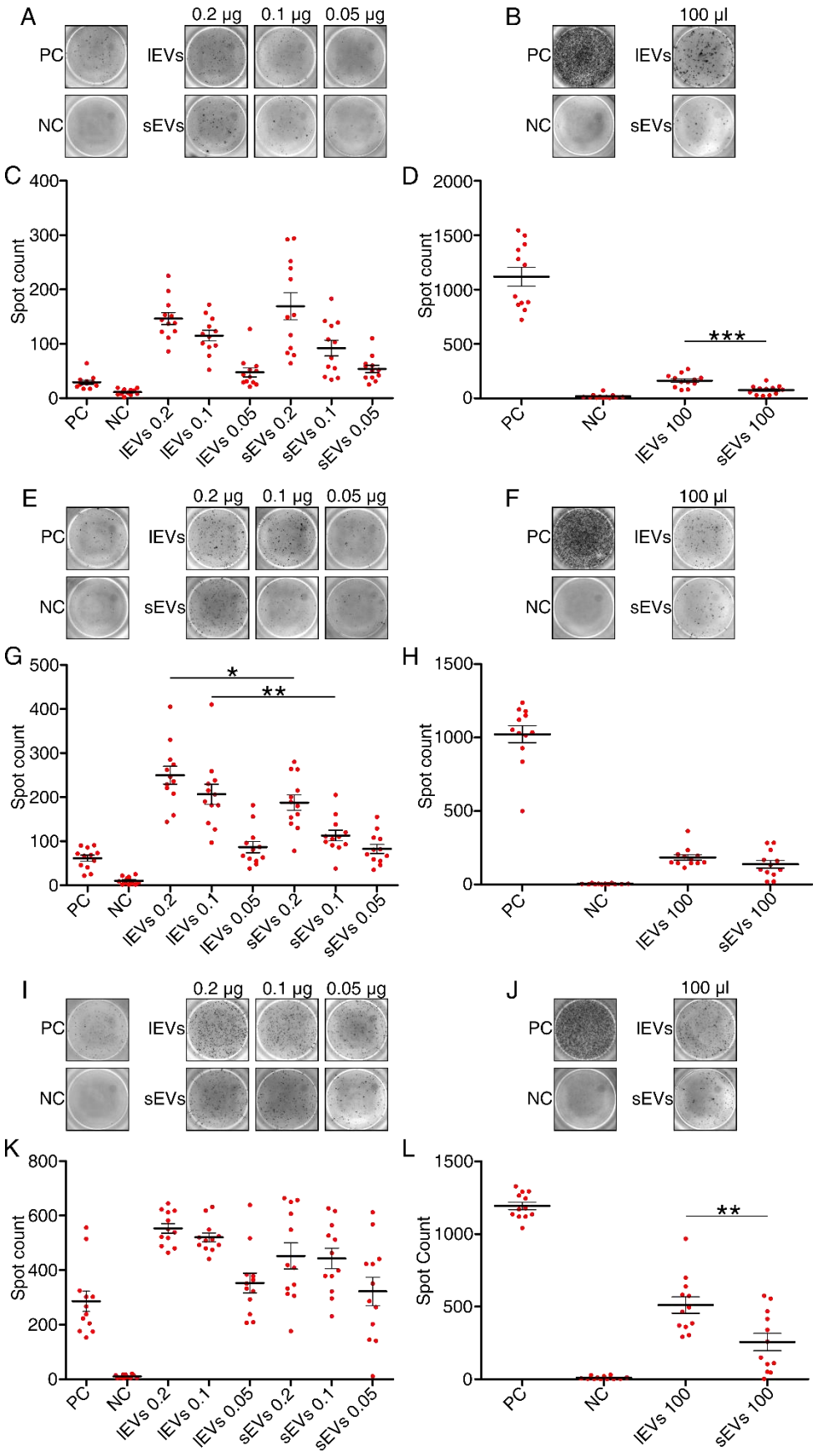
A
0.2 µg
0.1 µg
0.05 µg
PC
IEVs
NC
sEVs
B
100 µl
PC
IEVs
NC
sEVs
C
Spot count
400
300
200
100
0
PC
NC
IEVs 0.2
IEVs 0.1
IEVs 0.05
sEVs 0.2
sEVs 0.1
sEVs 0.05
D
Spot count
2000
1500
1000
500
0
***
PC
NC
IEVs 100
sEVs 100
E
0.2 µg
0.1 µg
0.05 µg
PC
IEVs
NC
sEVs
F
100 µl
PC
IEVs
NC
sEVs
G
Spot count
500
400
300
200
100
0
*
**
PC
NC
IEVs 0.2
IEVs 0.1
IEVs 0.05
sEVs 0.2
sEVs 0.1
sEVs 0.05
H
Spot count
1500
1000
500
0
PC
NC
IEVs 100
sEVs 100
I
0.2 µg
0.1 µg
0.05 µg
PC
IEVs
NC
sEVs
J
100 µl
PC
IEVs
NC
sEVs
K
Spot count
800
600
400
200
0
PC
NC
IEVs 0.2
IEVs 0.1
IEVs 0.05
sEVs 0.2
sEVs 0.1
sEVs 0.05
L
Spot Count
1500
1000
500
0
**
PC
NC
IEVs 100
sEVs 100

394

395 **Figure 7: Scrapie cell assay of CAD5 cells infected with EVs.** (a, e, i) Example images of wells in the scrapie cell assay infected
396 with the TPS scheme in passages 3 (a), 5 (e), and 8 (i). PC – positive control (infection by CAD5-RML cell homogenate), NC –
397 negative control (infection by CAD5 cell homogenate). A total of 1000 cells were transferred to each well. (b, f, j) Representative
398 images of wells in the scrapie cell assay infected with the OVS scheme in passages 3 (b), 5 (f), and 8 (j). A total of 10,000 cells
399 were transferred to each well. (c, g, k) Spot count in each well of the scrapie cell assay (hexaplicates of infection from a duplicate
400 of isolation) – TPS infection in passage 3 (c), 5 (g), and 8 (k). Each circle represents the count in one well. The thick line
401 represents the mean value with SEM, statistical significance was determined using an unpaired t-test ***$P < 0.001$ **$P < 0.01$
402 *$P < 0.05$. (d, h, l) Spot count in each well of the scrapie cell assay in OVS infection at passage 3 (d), 5 (h), and 8 (l). For
403 visualization purposes, all images were enhanced with brightness and contrast.

404 Discussion:

405 The presence of infectious prion protein in exosomes was demonstrated by Février et al. (14), which is
406 consistent with cellular prion conversion sites in the endolysosomal compartment, including MVBs (49,
407 50). However, one of the conversion sites of prion protein is the plasma membrane (55), and Mattei et
408 al. (58) found PrP^{TSE} in microvesicles. PrP^{TSE} can be transmitted via EVs in cell culture (52). According to
409 Godsave et al. (74), approximately 50% of PrP^{TSE} is on the cell surface, 30% in invaginations, and only
410 approximately 20% in cellular vesicles in the infected hippocampus. Although the predominant location
411 of PrP^{TSE} is on the cellular surface, no one has compared microvesicles and exosomes in the spread of
412 infection. To address this issue, we used a CAD5 cell model of prion infection infected with the RML prion
413 strain. As a second cell line, we chose N2a-PK1 cells. Although both cell lines were selected for high prion
414 production, CAD5 was produced by targeted oncogenesis of mouse catecholaminergic cells (75), and
415 N2a-PK1 was derived from mouse neuroblastoma cells (65). We tested the isolation protocol for
416 microvesicles and exosomes to collect enriched fractions of these vesicles. According to the International
417 Society of Extracellular Vesicles (ISEV) nomenclature and its position paper (76), we describe our
418 collected fractions as large EVs, pelleted at 20,000 × g and enriched in β-1 integrin, possibly
419 predominated by microvesicles. The sEVs were pelleted at 110,000 × g and enriched in CD9, CD63, TSG-
420 101, and Alix. This fraction should be predominated by exosomes. Although we optimized the isolation
421 procedure, we could not isolate the pure sEV fraction without β-1 integrin, which is one of the markers
422 for microvesicles (35), but it was recently also found in exosomes as another possible microvesicle
423 marker (36). This would explain the presence of β-1 integrin in our sEV fraction. Recently, Annexin A1

424 was found to be a specific marker for microvesicles (36). We found enrichment of CD9 tetraspanin in
425 sEVs compared to lEVs, as published previously (77). Based on the detection of β-1 integrin in the lEV
426 fraction, enrichment of CD9 in the sEV fraction compared to the lEV fraction, and no calnexin
427 contamination, we believe that our lEV fraction is predominated by microvesicles and the sEV fraction by
428 exosomes.

429 When we compared the EV fraction to the whole-cell lysate, we found great enrichment of both PrP^{TSE}
430 and PrP^{C}. The fraction of lEVs from CAD5 cells could not be isolated without contamination by calnexin
431 under the various centrifugations we tried during isolation optimization. Typically, the presence of
432 calnexin signals contamination from other cellular compartments (76). In our lEV and sEV fractions, there
433 was not a 100 kDa band of calnexin but three somewhat smaller bands that appeared in cells during
434 apoptosis (78), visible only after immense overexposure of the membrane (three times longer exposure
435 of the membrane or stretching of the histogram from 16 bit to 12 bit). Therefore, we assume that
436 apoptotic bodies could cause this contamination since they overlap in size.

437 Isolated fractions of EVs could be normalized in two possible ways. By total lipid concentration (79) or
438 total protein concentrations. Since we looked at prion protein transmission, we normalized EVs to
439 protein concentration using the BCA assay. Measurement of particle number in two fractions distinct in
440 size, which are heterogeneous, is problematic. Counting particles of different sizes by resistive pulse
441 sensing (RPS) did not yield reliable results. A fixed pore size is needed for reproducible measurement, yet
442 lEVs require a large pore size (80), with which sEVs are not detected (81). For NTA, this method has a
443 high relative concentration error for beads of 400 nm (82). The minimum sizes for measuring vesicles are
444 70-90 nm by NTA and 70-100 nm by RPS (82). In our sEV fraction, we detected the smallest particles with
445 a size of 30 nm by cryo-TEM. Furthermore, processing software may induce artifacts since the two
446 fractions need different settings (82).

447 We isolated both fractions from the same source, a conditioned medium, allowing us to compare these
448 fractions in PrP levels directly. The PrP PK- levels in lEVs and sEVs were relatively the same in the CAD5-
449 RML model, but in the N2a-PK1-RML model, the PrP PK- levels were slightly higher in lEVs. When we
450 looked at PrPres levels in CAD5 EVs, they were higher in sEVs. The difference in N2a-PK1 EVs was in the
451 opposite direction; the levels of PrPres were higher in lEVs. Our RT-QuIC experiments revealed higher
452 conversion activity in lEVs than in sEVs from both cell lines.

453 Next, we examined the infectivity of EVs by infecting native cells. First, we collected supernatants and
454 pellets from all steps of the isolation protocol to map the distribution of prion infectivity in the CAD5
455 model. As expected, all the fractions contained the infectivity, including the fractions of isolated EVs. In
456 accord with their higher RT-QuIC conversion activity, the lEVs caused approximately four times higher
457 CAD5 cell infection than sEVs in our initial cell blot experiments. We specifically looked at the difference
458 between EVs by two distinct approaches. The OVS scheme aimed to evaluate the differences in the
459 production of EVs by cells. Large EVs and sEVs were isolated from the same number of cells, and we
460 omitted the washing steps to eliminate the loss of EVs as much as possible. The TPS scheme aimed to
461 explore differences in the concentration of prion infectivity in washed vesicles and possibly also in their
462 uptake by the cells. With both infection schemes, we obtained concurrent results demonstrating higher
463 infectivity of lEVs in the CAD5 model. To overcome the limitations of cell blotting developed with alkaline
464 phosphatase, which is prone to signal saturation, we utilized fluorescent western blotting with greater
465 linear range of signal detection. The differences were even higher than in the cell blot. To further
466 demonstrate stronger infection by lEVs, we utilized SSCA to count number of infected cells directly.
467 Interestingly, in SSCA, we reached the infection plateau earlier (between the 5th and 8th passages)
468 compared to the cell blot and western blot (8th – 10th passages). In the fifth passage, we had
469 significantly more spots in TPS infection by lEVs. In OVS infection, we had significantly more spots in the

470 3rd and 8th passages in infection by lEVs. The differences measured by SSCA were less dramatic, but
471 consistent with the results of the cell and western blot analysis.

472 To confirm stronger infection by lEVs in the CAD5 model, we similarly tested the infection by EVs in the
473 N2a-PK1 cell line. Infection by lEVs was also stronger than that by sEVs with both infection schemes. In
474 CAD5 models, it is interesting to note that the TPS scheme infection led to a greater difference between
475 lEVs and sEVs suggesting higher concentration of the infectivity in lEVs. However, in the N2a-PK1 model,
476 the TPS infection scheme led only to small difference suggesting similar concentration of infectivity in
477 large and small EVs. In comparison, OVS infection scheme resulted in larger differences indicating
478 enhanced production of lEVs by N2a-PK1 cells. To purify sEVs from aggregated PrP (also pelleted at
479 110,000 × g), we introduced a sucrose cushion in the isolation of sEVs (83). Without the sucrose cushion
480 step, the measurement would be biased by pelleted PrP aggregates. The effectiveness of the cells
481 infection by lEVs and sEVs could be affected also by differences in their uptake. Since it is problematic to
482 separate microvesicles and exosomes, there is limited knowledge of the uptake of different fractions of
483 EVs. EVs can function as ligands for the surface receptor or be internalized by phagocytosis,
484 macropinocytosis, caveolin-mediated endocytosis, clathrin-mediated endocytosis, lipid raft-mediated
485 endocytosis, or fusion with the plasma membrane (32).

486 The CAD5 cells infected with the OVS scheme had a greater difference between infection levels in lEVs
487 and sEVs compared to the TPS scheme. Conversely, in N2a-PK1 cells, the TPS scheme resulted in a higher
488 discrepancy between infection levels in lEVs and sEVs compared to the OVS scheme. One possible
489 explanation could be in the cell origin. CAD5 is derived from Cath.a cells and has lost the immortalizing
490 oncogene (75). Cath.a cells secrete dopamine and norepinephrine (84), and cells secreting hormones and
491 neurotransmitters are specialized for secreting EVs (32). Conversely, the N2a-PK1 cell line is derived from
492 neuroblastoma Neuro 2A cells that produce low levels of tyrosine hydroxylase and dopamine unless they
493 are differentiated (85). It could be possible that the release of EVs is also specific to the cell type. The

494 RK13 lines, which express PrP^{C} from sheep, mice, or voles infected by different prion strains, release
495 PrP^{TSE} in exosomes differently (86).

496 Conclusion:

497 Prion protein is enriched in both large and small EVs. CAD5-RML lEVs contain higher prion converting
498 activity and infect native CAD5 cells more strongly than sEVs. We confirmed these results using three
499 different methods and two approaches to infection, one assessing the concentration of infectivity in
500 isolated EVs, and the second reflecting the total amount of infectivity associated with the EV fractions.
501 For validation, we used the N2a-PK1-RML cell line, in which we also achieved stronger infection by lEVs.
502 If the higher prion converting activity of lEVs was the sole reason why the infection with lEVs was
503 stronger remains to be elucidated since there is limited knowledge of the differences upon uptake of
504 different fractions of EVs. Small EVs or exosomes have been extensively studied compared to
505 microvesicles, yet microvesicles could play significant roles in other diseases, such as cancer or cellular
506 communication and immunity. Our data suggest the importance of lEVs in the trafficking of prions, which
507 should be considered in future prion transmission studies.

508 Declarations:

509 Ethics approval and consent to participate: Do not apply.

510 Consent of Publication: All authors agreed to publish the study.

511 Availability of data and material: We have submitted all relevant data of our experiments to the EV-
512 TRACK knowledgebase (EV-TRACK ID: EV220318). The original data are available at the BioImage Archive
513 repository (URL: https://www.ebi.ac.uk/biostudies/studies/S-BSST1019).

514 The authors declare no conflicts of interest.

The study was funded by Charles University projects GA UK 360216 and Cooperatio 207032-3 and The project National Institute for Neurological Research (Program EXCELES, ID Project No. LX22NPO5107) - Funded by the European Union – Next Generation EU.

Author Contributions: Conceptualization: Jakub Soukup, Methodology: Jakub Soukup, Cryo-electron Microscopy: Sami Kereïche, Jakub Soukup, RT-QuIC: Tibor Moško, writing – original draft: Jakub Soukup, writing – review and editing: Karel Holada, Sami Kereïche, Jakub Soukup, Funding: Jakub Soukup, Karel Holada.

Acknowledgment: The authors thank Charles Weissmann from The Scripps Research Institute (FL, USA) for providing the CAD5, Peter Klöhn from MRC Prion Unit (London, UK) for providing the N2a-PK1 cells, the TSE Resource Centre (Roslin Institute, UK) for providing the AH6 antibody, and Adriano Aguzzi (Institute of Neuropathology, University of Zurich, Switzerland) for kindly providing the RML5 scrapie strain. The TEM was performed in the Vinicna Microscopy Core Facility co-financed by the Czech-BioImaging large RI project LM2023050. Computational resources were supplied by the project "e-Infrastruktura CZ" (e-INFRA LM2018140) provided within the program Projects of Large Research, Development and Innovations Infrastructure.

References:

1. Colby DW, Prusiner SB. Prions. Cold Spring Harbor Perspectives in Biology. 2011;3(1).
2. Lawson VA, Collins SJ, Masters CL, Hill AF. Prion protein glycosylation. J Neurochem. 2005;93(4):793-801.
3. Kostelanska M, Freisleben J, Hanusova ZB, Mosko T, Vik R, Moravcova D, et al. Optimization of the photodynamic inactivation of prions by a phthalocyanine photosensitizer: The crucial involvement of singlet oxygen. J Biophotonics. 2019;12(8):13.
4. Stahl N, Borchelt DR, Hsiao K, Prusiner SB. Scrapie Prion Protein Contains a Phosphatidylinositol Glycolipid. Cell. 1987;51(2):229-40.
5. Riek R, Wider G, Billeter M, Hornemann S, Glockshuber R, Wuthrich K. Prion protein NMR structure and familial human spongiform encephalopathies. Proceedings of the National Academy of Sciences of the United States of America. 1998;95(20):11667-72.

542 6. Zahn R, Liu AZ, Luhrs T, Riek R, von Schroetter C, Garcia FL, et al. NMR solution structure of the
543 human prion protein. Proceedings of the National Academy of Sciences of the United States of America.
544 2000;97(1):145-50.
545 7. McKinley MP, Bolton DC, Prusiner SB. A protease-resistant protein is a structural component of
546 the Scrapie prion. Cell. 1983;35(1):57-62.
547 8. Gough KC, Maddison BC. Prion transmission Prion excretion and occurrence in the environment.
548 Prion. 2010;4(4):275-82.
549 9. McBride PA, Schulz-Schaeffer WJ, Donaldson M, Bruce M, Diringer H, Kretzschmar HA, et al. Early
550 spread of scrapie from the gastrointestinal tract to the central nervous system involves autonomic fibers
551 of the splanchnic and vagus nerves. Journal of Virology. 2001;75(19):9320-7.
552 10. Glaysher BR, Mabbott NA. Role of the GALT in scrapie agent neuroinvasion from the intestine.
553 Journal of Immunology. 2007;178(6):3757-66.
554 11. Brown KL, Stewart K, Ritchie DL, Mabbott NA, Williams A, Fraser H, et al. Scrapie replication in
555 lymphoid tissues depends on prion protein-expressing follicular dendritic cells. Nature Medicine.
556 1999;5(11):1308-12.
557 12. Kanu N, Imokawa Y, Drechsel DN, Williamson RA, Birkett CR, Bostock CJ, et al. Transfer of scrapie
558 prion infectivity by cell contact in culture. Curr Biol. 2002;12(7):523-30.
559 13. Gousset K, Schiff E, Langevin C, Marijanovic Z, Caputo A, Browman DT, et al. Prions hijack
560 tunnelling nanotubes for intercellular spread. Nature Cell Biology. 2009;11(3):328-U232.
561 14. Fevrier B, Vilette D, Archer F, Loew D, Faigle W, Vidal M, et al. Cells release prions in association
562 with exosomes. Proceedings of the National Academy of Sciences of the United States of America.
563 2004;101(26):9683-8.
564 15. Natale G, Ferrucci M, Lazzeri G, Paparelli A, Fornai F. Transmission of prions within the gut and
565 toward the central nervous system. Prion. 2011;5(3):142-9.
566 16. Sigurdson CJ, Bartz JC, Glatzel M. Cellular and Molecular Mechanisms of Prion Disease. Annu Rev
567 Pathol. 2019;14:497-516.
568 17. van Niel G, Carter DRF, Clayton A, Lambert DW, Raposo G, Vader P. Challenges and directions in
569 studying cell-cell communication by extracellular vesicles. Nat Rev Mol Cell Biol. 2022;23(5):369-82.
570 18. Colombo M, Raposo G, Thery C. Biogenesis, Secretion, and Intercellular Interactions of Exosomes
571 and Other Extracellular Vesicles. In: Schekman R, Lehmann R, editors. Annual Review of Cell and
572 Developmental Biology, Vol 30. Annual Review of Cell and Developmental Biology. 30. Palo Alto: Annual
573 Reviews; 2014. p. 255-89.
574 19. Henne WM, Buchkovich NJ, Emr SD. The ESCRT Pathway. Dev Cell. 2011;21(1):77-91.
575 20. Trajkovic K, Hsu C, Chiantia S, Rajendran L, Wenzel D, Wieland F, et al. Ceramide triggers budding
576 of exosome vesicles into multivesicular Endosomes. Science. 2008;319(5867):1244-7.
577 21. Heijnen HFG, Schiel AE, Fijnheer R, Geuze HJ, Sixma JJ. Activated platelets release two types of
578 membrane vesicles: Microvesicles by surface shedding and exosomes derived from exocytosis of
579 multivesicular bodies and alpha-granules. Blood. 1999;94(11):3791-9.
580 22. Buschow SI, Nolte-'t Hoen ENM, van Niel G, Pols MS, ten Broeke T, Lauwen M, et al. MHC II in
581 Dendritic Cells is Targeted to Lysosomes or T Cell-Induced Exosomes Via Distinct Multivesicular Body
582 Pathways. Traffic. 2009;10(10):1528-42.
583 23. Klumperman J, Raposo G. The Complex Ultrastructure of the Endolysosomal System. Cold Spring
584 Harbor Perspectives in Biology. 2014;6(10):22.
585 24. Hessvik NP, verbye A, Brech A, Torgersen ML, Jakobsen IS, Sandvig K, et al. PIKfyve inhibition
586 increases exosome release and induces secretory autophagy. Cellular and Molecular Life Sciences.
587 2016;73(24):4717-37.
588 25. Murrow L, Malhotra R, Debnath J. ATG12-ATG3 interacts with Alix to promote basal autophagic
589 flux and late endosome function. Nature Cell Biology. 2015;17(3):300-+.

590 26. Baietti MF, Zhang Z, Mortier E, Melchior A, Degeest G, Geeraerts A, et al. Syndecan-syntenin-ALIX
591 regulates the biogenesis of exosomes. Nature Cell Biology. 2012;14(7):677-85.
592 27. Kowal J, Arras G, Colombo M, Jouve M, Morath JP, Primdal-Bengtson B, et al. Proteomic
593 comparison defines novel markers to characterize heterogeneous populations of extracellular vesicle
594 subtypes. Proceedings of the National Academy of Sciences of the United States of America.
595 2016;113(8):E968-E77.
596 28. Wang J, Zhuang XJ, Greene KS, Si H, Antonyak MA, Druso JE, et al. Cdc42 functions as a regulatory
597 node for tumour-derived microvesicle biogenesis. Journal of Extracellular Vesicles. 2021;10(3):17.
598 29. Dai HJ, Zhang SS, Du XK, Zhang WK, Jing R, Wang XX, et al. RhoA inhibitor suppresses the
599 production of microvesicles and rescues high ventilation induced lung injury. Int Immunopharmacol.
600 2019;72:74-81.
601 30. Sun MJ, Xue XF, Li LY, Xu DD, Li SH, Li SWC, et al. Ectosome biogenesis and release processes
602 observed by using live-cell dynamic imaging in mammalian glial cells. Quant Imaging Med Surg.
603 2021;11(11):4604-16.
604 31. Nabhan JF, Hu RX, Oh RS, Cohen SN, Lu Q. Formation and release of arrestin domain-containing
605 protein 1-mediated microvesicles (ARMMs) at plasma membrane by recruitment of TSG101 protein.
606 Proceedings of the National Academy of Sciences of the United States of America. 2012;109(11):4146-51.
607 32. van Niel G, D'Angelo G, Raposo G. Shedding light on the cell biology of extracellular vesicles. Nat
608 Rev Mol Cell Biol. 2018;19(4):213-28.
609 33. Andreu Z, Yanez-Mo M. Tetraspanins in extracellular vesicle formation and function. Front
610 Immunol. 2014;5:12.
611 34. Laghezza Masci V, Taddei AR, Gambellini G, Giorgi F, Fausto AM. Microvesicles shed from
612 fibroblasts act as metalloproteinase carriers in a 3-D collagen matrix. J Circ Biomark.
613 2016;5:1849454416663660.
614 35. Momen-Heravi F, Getting SJ, Moschos SA. Extracellular vesicles and their nucleic acids for
615 biomarker discovery. Pharmacol Ther. 2018;192:170-87.
616 36. Jeppesen DK, Fenix AM, Franklin JL, Higginbotham JN, Zhang Q, Zimmerman LJ, et al.
617 Reassessment of Exosome Composition. Cell. 2019;177(2):428-+.
618 37. Deleo AM, Ikezu T. Extracellular Vesicle Biology in Alzheimer's Disease and Related Tauopathy. J
619 Neuroimmune Pharm. 2018;13(3):292-308.
620 38. Bobrie A, Colombo M, Krumeich S, Raposo GA, Thery C. Diverse subpopulations of vesicles
621 secreted by different intracellular mechanisms are present in exosome preparations obtained by
622 differential ultracentrifugation. Journal of Extracellular Vesicles. 2012;1(1):11.
623 39. Zhang HY, Freitas D, Kim HS, Fabijanic K, Li Z, Chen HY, et al. Identification of distinct
624 nanoparticles and subsets of extracellular vesicles by asymmetric flow field-flow fractionation. Nature
625 Cell Biology. 2018;20(3):332-+.
626 40. Sunyach C, Jen A, Deng J, Fitzgerald KT, Frobert Y, Grassi J, et al. The mechanism of
627 internalization of glycosylphosphatidylinositol-anchored prion protein. Embo Journal. 2003;22(14):3591-
628 601.
629 41. Sarnataro D, Campana V, Paladino S, Stornaiuolo M, Nitsch L, Zurzolo C. PrPC association with
630 lipid rafts in the early secretory pathway stabilizes its cellular conformation. Molecular Biology of the
631 Cell. 2004;15(9):4031-42.
632 42. Fremuntova Z, Mosko T, Soukup J, Kucerova J, Kostelanska M, Hanusova ZB, et al. Changes in
633 cellular prion protein expression, processing and localisation during differentiation of the neuronal cell
634 line CAD 5. Biology of the Cell. 2020;112(1):1-21.
635 43. Brouckova A, Holada K. Cellular prion protein in blood platelets associates with both lipid rafts
636 and the cytoskeleton. Thromb Haemost. 2009;102(5):966-74.
637 44. Didonna A. Prion protein and its role in signal transduction. Cell Mol Biol Lett. 2013;18(2):209-30.

638 45. Shyng SL, Huber MT, Harris DA. A Prion Protien Cycles Between the Cell-surface and an Endocytic
639 Compartment in Cultured Neuroblastoma-Cells. Journal of Biological Chemistry. 1993;268(21):15922-8.
640 46. Peters PJ, Mironov A, Peretz D, van Donselaar E, Leclerc E, Erpel S, et al. Trafficking of prion
641 proteins through a caveolae-mediated endosomal pathway. J Cell Biol. 2003;162(4):703-17.
642 47. Yim YI, Park BC, Yadavalli R, Zhao XH, Eisenberg E, Greene LE. The multivesicular body is the
643 major internal site of prion conversion. J Cell Sci. 2015;128(7):1434-43.
644 48. Guo BB, Bellingham SA, Hill AF. The Neutral Sphingomyelinase Pathway Regulates Packaging of
645 the Prion Protein into Exosomes. Journal of Biological Chemistry. 2015;290(6):3455-67.
646 49. Veith NM, Plattner H, Stuermer CAO, Schulz-Schaeffer WJ, Burkle A. Immunolocalisation of PrPSc
647 in scrapie-infected N2a mouse neuroblastoma cells by light and electron microscopy. Eur J Cell Biol.
648 2009;88(1):45-63.
649 50. Marijanovic Z, Caputo A, Campana V, Zurzolo C. Identification of an Intracellular Site of Prion
650 Conversion. Plos Pathogens. 2009;5(5):15.
651 51. Vilette D, Laulagnier K, Huor A, Alais S, Simoes S, Maryse R, et al. Efficient inhibition of infectious
652 prions multiplication and release by targeting the exosomal pathway. Cellular and Molecular Life
653 Sciences. 2015;72(22):4409-27.
654 52. Guo BB, Bellingham SA, Hill AF. Stimulating the Release of Exosomes Increases the Intercellular
655 Transfer of Prions. Journal of Biological Chemistry. 2016;291(10):5128-37.
656 53. Vella LJ, Sharples RA, Lawson VA, Masters CL, Cappai R, Hill AF. Packaging of prions into
657 exosomes is associated with a novel pathway of PrP processing. Journal of Pathology. 2007;211(5):582-
658 90.
659 54. D'Arrigo G, Gabrielli M, Scaroni F, Swuec P, Amin L, Pegoraro A, et al. Astrocytes-derived
660 extracellular vesicles in motion at the neuron surface: Involvement of the prion protein. Journal of
661 Extracellular Vesicles. 2021;10(9):22.
662 55. Goold R, Rabbanian S, Sutton L, Andre R, Arora P, Moonga J, et al. Rapid cell-surface prion
663 protein conversion revealed using a novel cell system. Nat Commun. 2011;2.
664 56. Yamasaki T, Baron GS, Suzuki A, Hasebe R, Horiuchi M. Characterization of intracellular dynamics
665 of inoculated PrP-res and newly generated PrPSc during early stage prion infection in Neuro2a cells.
666 Virology. 2014;450:324-35.
667 57. Goold R, McKinnon C, Rabbanian S, Collinge J, Schiavo G, Tabrizi SJ. Alternative fates of newly
668 formed PrPSc upon prion conversion on the plasma membrane. J Cell Sci. 2013;126(16):3552-62.
669 58. Mattei V, Barenco MG, Tasciotti V, Garofalo T, Longo A, Boller K, et al. Paracrine Diffusion of PrPC
670 and Propagation of Prion Infectivity by Plasma Membrane-Derived Microvesicles. Plos One. 2009;4(4).
671 59. Saa P, Yakovleva O, de Castro J, Vasilyeva I, De Paoli SH, Simak J, et al. First Demonstration of
672 Transmissible Spongiform Encephalopathy-associated Prion Protein (PrPTSE) in Extracellular Vesicles
673 from Plasma of Mice Infected with Mouse-adapted Variant Creutzfeldt-Jakob Disease by in Vitro
674 Amplification. Journal of Biological Chemistry. 2014;289(42):29247-60.
675 60. Cervenakoya L, Saa P, Yakoyleva O, Vasilyeva I, de Castro J, Brown P, et al. Are prions transported
676 by plasma exosomes? Transfusion and Apheresis Science. 2016;55(1):70-83.
677 61. Saa P. Is sporadic Creutzfeldt-Jakob disease transfusion-transmissible? Transfusion.
678 2020;60(4):655-8.
679 62. Benmoussa A, Lee CHC, Laffont B, Savard P, Laugier J, Boilard E, et al. Commercial Dairy Cow Milk
680 microRNAs Resist Digestion under Simulated Gastrointestinal Tract Conditions. J Nutr.
681 2016;146(11):2206-15.
682 63. Rahman MM, Shimizu K, Yamauchi M, Takase H, Ugawa S, Okada A, et al. Acidification effects on
683 isolation of extracellular vesicles from bovine milk. Plos One. 2019;14(9):12.

684 64. Mahal SP, Baker CA, Demczyk CA, Smith EW, Julius C, Weissmann C. Prion strain discrimination in
685 cell culture: The cell panel assay. Proceedings of the National Academy of Sciences. 2007;104(52):20908-
686 13.
687 65. Klohn PC, Stoltze L, Flechsig E, Enari M, Weissmann C. A quantitative, highly sensitive cell-based
688 infectivity assay for mouse scrapie prions. Proceedings of the National Academy of Sciences of the
689 United States of America. 2003;100(20):11666-71.
690 66. Van Deun J, Mestdagh P, Agostinis P, Akay Ö, Anand S, Anckaert J, et al. EV-TRACK: transparent
691 reporting and centralizing knowledge in extracellular vesicle research. Nature Methods. 2017;14(3):228-
692 32.
693 67. Théry C, Amigorena S, Raposo G, Clayton A. Isolation and Characterization of Exosomes from Cell
694 Culture Supernatants and Biological Fluids. Current Protocols in Cell Biology. 2006;30(1):3.22.1-3..9.
695 68. Janouskova O, Rakusan J, Karaskova M, Holada K. Photodynamic inactivation of prions by
696 disulfonated hydroxyaluminium phthalocyanine. Journal of General Virology. 2012;93:2512-7.
697 69. Foutz A, Appleby BS, Hamlin C, Liu XQ, Yang S, Cohen Y, et al. Diagnostic and prognostic value of
698 human prion detection in cerebrospinal fluid. Ann Neurol. 2017;81(1):79-92.
699 70. Mosko T, Galuskova S, Matej R, Buzova M, Holada K. Detection of Prions in Brain Homogenates
700 and CSF Samples Using a Second-Generation RT-QuIC Assay: A Useful Tool for Retrospective Analysis of
701 Archived Samples. Pathogens. 2021;10(6):13.
702 71. Hanusova Z, Mosko T, Matej R, Holada K. Precision in the design of an experimental study
703 deflects the significance of proteinase-activated receptor 2 expression in scrapie-inoculated mice.
704 Journal of General Virology. 2017;98(6):1563-9.
705 72. Soukup J, Kostelanska M, Kereiche S, Hujacova A, Pavelcova M, Petrak J, et al. Flow Cytometry
706 Analysis of Blood Large Extracellular Vesicles in Patients with Multiple Sclerosis Experiencing Relapse of
707 the Disease. J Clin Med. 2022;11(10):15.
708 73. Dubochet J, Adrian M, Chang JJ, Homo JC, Lepault J, McDowall AW, et al. Cryo-electron
709 microscopy of vitrified specimens. Q Rev Biophys. 1988;21(2):129-228.
710 74. Godsave SF, Wille H, Pierson J, Prusiner SB, Peters PJ. Plasma membrane invaginations containing
711 clusters of full-length PrPSc are an early form of prion-associated neuropathology in vivo. Neurobiol
712 Aging. 2013;34(6):1621-31.
713 75. Qi YP, Wang JKT, McMillian M, Chikaraishi DM. Characterization of a CNS cell line, CAD, in which
714 morphological differentiation is initiated by serum deprivation. J Neurosci. 1997;17(4):1217-25.
715 76. Thery C, Witwer KW, Aikawa E, Alcaraz MJ, Anderson JD, Andriantsitohaina R, et al. Minimal
716 information for studies of extracellular vesicles 2018 (MISEV2018): a position statement of the
717 International Society for Extracellular Vesicles and update of the MISEV2014 guidelines. Journal of
718 Extracellular Vesicles. 2018;7(1):43.
719 77. Mathieu M, Nevo N, Jouve M, Valenzuela JI, Maurin M, Verweij FJ, et al. Specificities of exosome
720 versus small ectosome secretion revealed by live intracellular tracking of CD63 and CD9. Nat Commun.
721 2021;12(1):18.
722 78. Takizawa T, Tatematsu C, Watanabe K, Kato K, Nakanishi Y. Cleavage of calnexin caused by
723 apoptotic stimuli: Implication for the regulation of apoptosis. J Biochem(Tokyo). 2004;136(3):399-405.
724 79. Osteikoetxea X, Balogh A, Szabó-Taylor K, Németh A, Szabó TG, Pálóczi K, et al. Improved
725 Characterization of EV Preparations Based on Protein to Lipid Ratio and Lipid Properties. PLOS ONE.
726 2015;10(3):e0121184.
727 80. de Vrij J, Maas SL, van Nispen M, Sena-Esteves M, Limpens RW, Koster AJ, et al. Quantification of
728 nanosized extracellular membrane vesicles with scanning ion occlusion sensing. Nanomedicine (Lond).
729 2013;8(9):1443-58.

730 81. Coumans FAW, van der Pol E, Böing AN, Hajji N, Sturk G, van Leeuwen TG, et al. Reproducible
731 extracellular vesicle size and concentration determination with tunable resistive pulse sensing. Journal of
732 Extracellular Vesicles. 2014;3(1):25922.
733 82. van der Pol E, Coumans FA, Grootemaat AE, Gardiner C, Sargent IL, Harrison P, et al. Particle size
734 distribution of exosomes and microvesicles determined by transmission electron microscopy, flow
735 cytometry, nanoparticle tracking analysis, and resistive pulse sensing. J Thromb Haemost.
736 2014;12(7):1182-92.
737 83. Morales R, Hu PP, Duran-Aniotz C, Moda F, Diaz-Espinoza R, Chen B, et al. Strain-dependent
738 profile of misfolded prion protein aggregates. Sci Rep. 2016;6(1):20526.
739 84. Suri C, Fung BP, Tischler AS, Chikaraishi DM. Catecholaminergic cell lines from the brain and
740 adrenal glands of tyrosine hydroxylase-SV40 T antigen transgenic mice. J Neurosci. 1993;13(3):1280-91.
741 85. Tremblay RG, Sikorska M, Sandhu JK, Lanthier P, Ribecco-Lutkiewicz M, Bani-Yaghoub M.
742 Differentiation of mouse Neuro 2A cells into dopamine neurons. J Neurosci Methods. 2010;186(1):60-7.
743 86. Arellano-Anaya ZE, Huor A, Leblanc P, Lehmann S, Provansal M, Raposo G, et al. Prion strains are
744 differentially released through the exosomal pathway. Cellular and Molecular Life Sciences.
745 2015;72(6):1185-96.